Supporting Information

Lüer et al. 10.1073/pnas.1113080109

SI Text

Sample Preparation. Cells of *Rhodopseudomonas palustris* strain 2.1.6 were grown anaerobically in C-succinate medium at 30 °C in flat-sided glass bottles. The cultures were placed at different distances away from the incandescent bulbs so the intensity of light illuminating the cell culture could be varied from 220 lux for high light (HL) to 10 lux for low light (LL). To minimize any self-shading caused by the cells themselves, the cultures were regularly transferred into fresh media, thereby ensuring a constant low culture optical density. The cells were harvested by centrifugation (relative centrifugal field, $r_{AV} = 1{,}248 \times g$, 30 min), and resuspended and homogenized in 20 mM MES buffer, pH 6.8, containing 100 mM KCl. Cell pellet was resuspended in 20 mM Tris•HCl, pH 8.0, and the concentration was adjusted to give absorption of 70 cm^{-1} at 850 nm for HL membranes and at 800 nm for LL membranes. Afterward, the resuspended cells were broken by three passages through a French press (9,500 psi) in the presence of DNase and $MgCl_2$. Contaminants were removed first by centrifugation at $r_{AV} = 16{,}000 \times g$ for 10 min, then the photosynthetic membranes were pelleted by centrifugation at $r_{AV} = 184{,}000 \times g$ for 2 h. Concentrated membranes were stored at −20 °C until used for measurements. Prior to measurements, the samples were thawed and diluted in Tris•HCl buffer to reach $OD_{800} \sim 1$ in 1 mm quartz cuvettes. Samples with "closed" reaction center (RC) were prepared from membranes with "open" RC by addition of 1 mM sodium dithionite dissolved in 100 mM Tris•HCl buffer to reach final concentration 0.02 mM, and then measured.

Derivative Spectroscopy for Transient Absorption Measurements in Linear or Circular Aggregates. The extraction of population information from pump-probe kinetics is complicated by the strong spectral superposition of the transitions from the bacteriochlorophyll rings B850 and B875, which are only 40 meV apart, compared to their FWHM of approximately 70 meV. Both B850 and B875 display excitonic behavior, characteristic of linear and circular molecular aggregates. Their transient absorption (TA) spectrum consists of a ground-state photobleaching (PB) band and a blue-shifted photoinduced absorption (PA) band, due to the exciton-to-biexciton transition. The energetic splitting between PB and PA is rather small and depends on the degree of exciton delocalization (1, 2). In principle it would be possible to fit the TA spectra by the superposition of six bands (corresponding to PB and PA of B850LE, B850HE, and B875) but this would require a very large number of parameters, leading to uncertainties on the extracted populations and dynamics. Here we introduce an alternative procedure, relying on the frequency derivatives of the TA spectra, which allows us to directly access the B850 and B875 populations. Our approach is similar to derivative spectroscopy, which is a well-assessed technique for separation and quantitative analysis of overlapping bands in stationary absorption spectra (3, 4). Here we extend the method to TA spectra.

Let us consider a singly peaked symmetric bell-shaped function, such as a Gaussian or a Lorentzian. Its second derivative consists of two side maxima and a central minimum, with higher absolute intensity, at the same position as the peak of the original function, but with a significantly reduced width, which is simply caused by the fact that the second derivative is zero where the original function has its inflection points—i.e., at about half the original bandwidth or even less for Lorentzians. In the case of an absorption spectrum consisting of several adjacent peaks, building its second derivative will narrow their widths and thus facilitate their separation and assignment. We now consider an excitonic transition, with ground-state absorption described by a Lorentzian function centered at ω_0 and with FWHM w, $A(\omega - \omega_0) = \frac{A_0}{1+[\frac{2(\omega-\omega_0)}{w}]^2}$. The corresponding TA spectrum consists of a negative band centered at ω_0, corresponding to the PB of the ground-state absorption, and a blue-shifted positive band (centered at $\omega_0 + \Delta\omega$), corresponding to exciton-to-biexciton PA. One can thus write $\Delta A \approx A(\omega - \omega_0 - \Delta\omega) - A(\omega - \omega_0)$. If one assumes that the shift between PB and PA bands is much smaller than their width ($\Delta\omega \ll \omega$) then one can approximate $\Delta A \approx -dA/d\omega \cdot \Delta\omega$, showing that the TA spectrum is proportional to the first derivative of the ground-state absorption spectrum with respect to frequency. Hence, $d(\Delta A)/d\omega \approx -d^2A/d\omega^2 \cdot \Delta\omega$; i.e., the first derivative of the TA spectrum is to a first approximation proportional to the second derivative of the ground-state absorption. This fact allows us to exploit the method of derivative spectroscopy to alleviate the problem of spectral congestion, enabling separation of the different excitonic transitions and evaluation of their relative population.

To illustrate our method, we simulate two Lorentzian transitions with peak position and width corresponding to the B850 and B875 in HL *R. palustris*, as a function of the B875 relative concentration $r = A_0^{B875}/(A_0^{B850} + A_0^{B875})$. Fig. S1*A* shows the steady-state absorption spectra $A(\omega)$ as a function of r (black solid line in Fig. S1*B* shows the spectrum at $r = 0.5$, and red/green dashed lines its two components) which display a slight red shift for increasing r. Fig. S1*B* shows the first derivative $dA/d\omega$, which corresponds to the TA spectrum. One observes the presence of a positive and a negative peak, with the isosbestic point slightly shifting to the red for increasing r, showing that the TA spectra do not allow a direct assessment of the relative weights of the two moieties without fitting. Finally, Fig. S1*C* shows the second derivative spectra $d^2A/d\omega^2$; now two negative narrow peaks are clearly resolved at 1.4 ad 1.44 eV, allowing direct assessment of the relative B875 to B850 population by visual inspection. In *Results and Discussion* of the main article, we will therefore present the first derivatives of TA spectra, $d(\Delta A)/d\omega$.

Numerical Modeling of the Dynamics of the First Derivatives of TA Spectra. The numerical modeling followed a two-step procedure. First, we modeled the $d(\Delta A)/d\omega$ spectra with the superposition of three second derivatives of Voigt band shapes: one for the B875, and one for the B850 LE and HE excitons, peaking around 1.4, 1.45, and 1.50 eV, respectively. We found that the bandwidths of the different transitions did not vary significantly with pump-probe delay and pump energy, but were depending on sample type, so they were kept fixed for each sample during the fit and only the amplitudes and the spectral positions were allowed to vary. In a second step, the time-dependent spectral weights previously obtained were fit assuming a simple homogeneous reaction scheme involving three processes: the forward energy transfer (ET) B850 → B875, backward ET B850 ← B875, and B875 deactivation. We assume that the absorption cross-sections of both B875 and B850 are the same. In order to account for a small contribution of exciton annihilation of B850 excitons to the decay kinetics, a bimolecular decay path was also introduced (see *Exciton Annihilation in LL and HL Samples* below).

Ground-State Absorption and TA Spectra of Light-Harvesting Complex 2 (LH2). In Fig. S2*A*, we show a multi-Voigt analysis of the ground-state absorption spectrum of isolated LH2 complexes in their HL

form. Because in these spectra, B875 is not present and B850HE is weak, the contributions from B800 and B850 are well separated and can be reliably fitted. We found that the integrated spectral weights of the lowest energetic electronic transitions present a ratio $r = \mathrm{B800}/(\mathrm{B850HE} + \mathrm{B850LE}) = 0.544$. This ratio is close to the one expected from the molecule number ratio B800/B850 (9:18) if there were as little excitonic interaction in B850 as in B800. As a consequence, we conclude that a change in the excitonic interaction, when going from HL to LL, will lead to negligible change of this ratio. Furthermore, the B875 molecules in LH1, if present, will couple very little to the B850 molecules in LH2. This information is important because it allows us to fix the ratio $\mathrm{B800}/(\mathrm{B850LE} + \mathrm{B850HE})$ in all fits of ground-state absorption spectra of the HL and LL membranes to 0.544.

In order to test the applicability of our derivative approach, we verified our assumption that the TA spectra can be modeled by the superposition of positive and negative Lorentzian peaks, with frequency shifts much smaller than their widths, and peak position and width constant over time. To this purpose, we studied the B850 peak from isolated LH2 complexes of *R. palustris* in solution. Fig. S2 shows ΔA spectra of HL- and LL-grown samples (panels *B* and *C*, respectively) for an excitation energy of 1.48 eV, resonant with B850. In both cases, we were able to fit the time-dependent TA spectra by a superposition of one negative and one positive Lorentzian function, representing the PB and PA contributions. Free parameters were the frequency shift $\Delta\omega$ between PA and PB (Fig. S2*D*), the Lorentzian width w, assumed equal for both PA and PB (Fig. S2*E*), and the spectral weight of PA relative to PB. This simple model yields excellent fits for HL and still good fits for LL samples, if one considers the very low noise in the measurements, evidencing even the slightest deviations of the fitting curve from the data points. We found that the spectral weight of PA is 100% (90%) of that of PB for HL (LL) samples for all time delays. The facts that the offset $\Delta\omega$ is much smaller than the width w and that PA and PB have nearly equal spectral weights, for both HL and LL samples, justify our approximation of the TA spectrum as the first derivative of ground-state absorption. Fig. S2*D* shows that, for times >2 ps, the offset $\Delta\omega$ is constant for both HL and LL samples. This observation is very important, and is not usually displayed in this clarity by similar studies, because it is the prerequisite for time-invariant effective absorption cross-sections (defined as the sum of the cross-sections for PA and PB, respectively, at a certain wavelength). As pointed out by Novoderezkhin et al. (2), the observed intensity in the TA spectrum is a strong function of the overlap between PA and PB. Hence, in order to ascribe TA kinetics at a certain wavelength to population dynamics, rather than to a change in cross-sections, the latter must be demonstrated to be time invariant, which is shown to be the case in Fig. S2*D*. In Fig. S2*E*, we demonstrate that also the bandwidths are constant to within 2% in HL and LL for $t > 2$ ps, allowing us to extract population information not only from the ΔA spectra directly, but also from their first derivatives with respect to probe energy.

Exciton Annihilation in LL and HL Samples. In order to assess the influence of exciton annihilation on the forward and backward ET constants which are the focus of this paper, we varied the pump intensity over nearly three orders of magnitude, from 600 $\mathrm{nJ/cm^2}$ up to 300 $\mu\mathrm{J/cm^2}$. The measured TA spectra were treated as explained in the main text, to obtain the time-resolved populations of B850 and B875 excitons. Because in our measurements, exciton annihilation contributes only weakly to the overall dynamics, we modeled it in the simplest possible way, as a homogeneous bimolecular reaction according to

$$dc/dt = -k_{\mathrm{bi}}c^2, \qquad \textbf{[S1]}$$

where c is the concentration of B850 excitons. With our method, we do not obtain the absolute exciton concentration, but a quantity which is proportional to it, $p = r \cdot c$. Here, r is an unknown proportionality constant, which is however the same for B850 and B875 excitons. We can thus substitute c with p in Eq. **S1**:

$$dp/dt = -k_A p^2; \qquad k_A = k_{\mathrm{bi}}/r. \qquad \textbf{[S2]}$$

This rate equation has an analytical solution

$$p(t) = [1/p_0 + k_A t]^{-1}; \qquad p_0 = p(t=0). \qquad \textbf{[S3]}$$

For a bimolecular reaction, it is typical that the half-lifetime $t_{1/2}$, where $p(t)$ has decayed to half of p_0, depends on p_0:

$$t_{1/2} = [p_0 k_A]^{-1}. \qquad \textbf{[S4]}$$

In our experiment, monomolecular decay paths, with overall rate k_m, compete with the bimolecular decay:

$$dp/dt = -k_A p^2 - k_m p. \qquad \textbf{[S5]}$$

If we model only the early part of the decay, where $p(t) \approx p_0$, we can write

$$dp/dt = -k'_A p - k_m p; \qquad k'_A = k_A \cdot p_0. \qquad \textbf{[S6]}$$

A comparison with **[S4]** shows that $k'_A = 1/t_{1/2}$. The early kinetics, as long as $p(t) \approx p_0$, are thus given by

$$p(t) = p_0 \cdot \exp[-(k_m + 1/t_{1/2})t], \qquad \textbf{[S7]}$$

We can therefore obtain both k_m and $t_{1/2}$ by fitting exponential decay curves to the initial portion of the B850 exciton dynamics measured at various pump intensities (in reality, this has been done with a global fitting routine considering all probe wavelengths at the same time) and plotting the initial decay constant $k_i = k_m + k'_A$ as a function of p_0. We expect a straight line with slope k_A and a y-axis intersection k_m:

$$k_i = k_A \cdot p_0 + k_m. \qquad \textbf{[S8]}$$

Fig. S3*A* shows initial rate constants, as obtained from a series of measurements in HL and LL membranes at different pumping intensities, after pumping at 1.6 eV, into B800. To make these measurements comparable to the ones of the main manuscript where different pumping energies have been used, we represent the data not as function of the light intensity but as function of p_0, the initial B850 population. Our simple model of exciton annihilation depends only upon the initial population p_0 of B850 excitons, but not on how they have been generated (Markovian kinetics). We find that, in agreement with Eq. **S8**, the data points can be fitted by straight lines for both HL and LL samples, from which y-axis intersection and slope can be extracted with reasonable precision. Satisfyingly, the y-axis intersection, representing the monomolecular decay in the absence of exciton annihilation, is similar within 20% for both HL and LL samples. This behavior is expected because monomolecular deactivation involves nearly exclusively the B875 moiety, which is the same for LL and HL. The slopes are proportional to the bimolecular rate constant. It is obvious that bimolecular exciton annihilation is much stronger in HL than in LL samples, pointing to much slower exciton diffusion in LL than in HL, because bimolecular annihilation is mediated by B850 → B850 energy transfer steps. We use this important observation in the main text to justify the long memory of the excitation energy that occurs only in LL samples: The reduced exciton mobility in LL B850 complexes does not allow the excitons, initially formed on B875, to reach a different B875 during their lifetime. Excitons always return to the original B875 complex, thus retaining the memory of its particular site energy.

In order to represent bimolecular recombination by a useful quantity, we show in Fig. S3*B* the half-lifetimes, as obtained from the fits in Fig. S3*A*. The squares refer to the half-lifetimes, as obtained from the slopes of the straight lines from Fig. S3*A*. The solid lines refer to the same set of intensity dependent measurements, but are obtained by numerical modeling of the full kinetics, including bimolecular recombination (Eq. **1** in the main text) using a bimolecular reaction constant k_A which is valid for all intensities (global fitting of all probe energies, all intensities and all delay times with the same k_A). We find that these improved half-lifetimes are about a factor of two lower than the approximate ones, obtained from the fitting of the early decay phase, which is caused by an underestimation of bimolecular decay by a violation of the necessary condition for Eq. **S6** to hold. Obviously, when fitting early decay traces, the uncertainty in the initial slope becomes too large if the time range is too short, so a compromise must be found between respecting Eq. **S6** and keeping uncertainty to a reasonable level. In the range of intensities applied in the main text, we thus obtain bimolecular half-lifetimes of around 100 ps for HL and around 500 ps for LL measurements. We can therefore conclude that, in our measurements of the main text, bimolecular annihilation in HL membranes is strong enough that it needs to be considered, although it is virtually absent in LL membranes.

In Fig. S3*B*, we also show the half-life times of the measurements that yield the values in Table 1 of the main text (star-shaped symbols). Note that these measurements have only been done at a single intensity each, so the fitted bimolecular half-lifetimes rely only on the shape of the B850 decay kinetics but not on the intensity dependence. Still, we observe reasonable agreement for HL samples (black stars) with the trend of the intensity dependent measurements; this is not true for LL samples and simply reflects the fact that bimolecular annihilation in these samples is so weak that it cannot be reasonably fitted by considering only the shape of the decay dynamics at a single intensity.

In conclusion, we have quantified exciton annihilation in HL and LL samples. In LL samples, we found that annihilation is so weak that it will have no influence on the forward and backward ET constants reported in Table 1, whereas in HL samples, we showed that exciton annihilation must be considered, and we managed to quantify its influence.

1. Van Burgel M, Wiersma DA, Duppen K (1995) The dynamics of one-dimensional excitons in liquids. *J Chem Phys* 102:20–33.
2. Novoderezhkin V, Monshouwer R, van Grondelle R (1999) Exciton (de)localization in the LH2 antenna of *Rhodobacter sphaeroides* as revealed by relative difference absorption measurements of the LH2 antenna and the B820 subunit. *J Phys Chem B* 103:10540–10548.
3. Talsky G (1994) *Derivative Spectrophotometry* (VCH, Weinheim, Germany), 1st Ed.
4. Antonov L, Nedeltcheva D (2000) Resolution of overlapping UV-vis absorption bands and quantitative analysis. *Chem Soc Rev* 29:217–227.

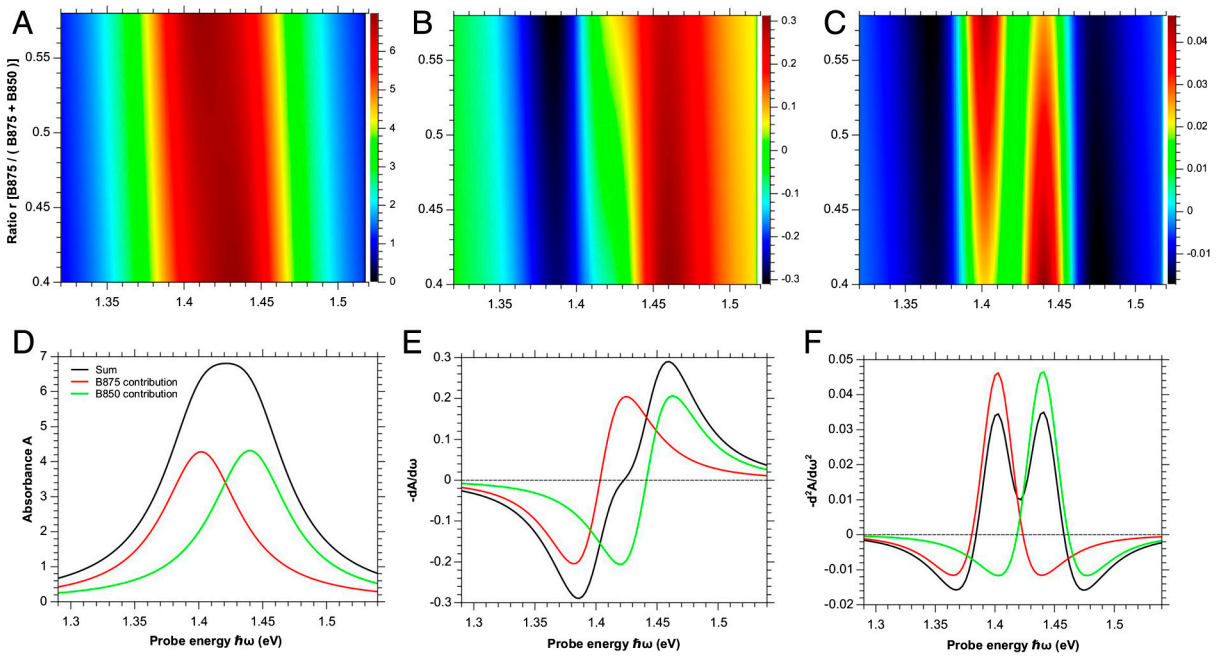

Fig. S1. Calculated spectra of B850 and B875 excitons at a population ratio varying from 0.4 to 0.6 (upper row) and at a fixed population ratio of 0.5, together with the isolated contributions from B850 and B875 (lower row, black, green, and red curves, respectively). The left column shows the spectra as calculated from a superposition of two Lorentzian functions, centered at 1.40 and 1.44 eV from B875 and B850, respectively, with a width of 70 meV each. The middle and right columns give the first and second derivative with respect to energy, respectively.

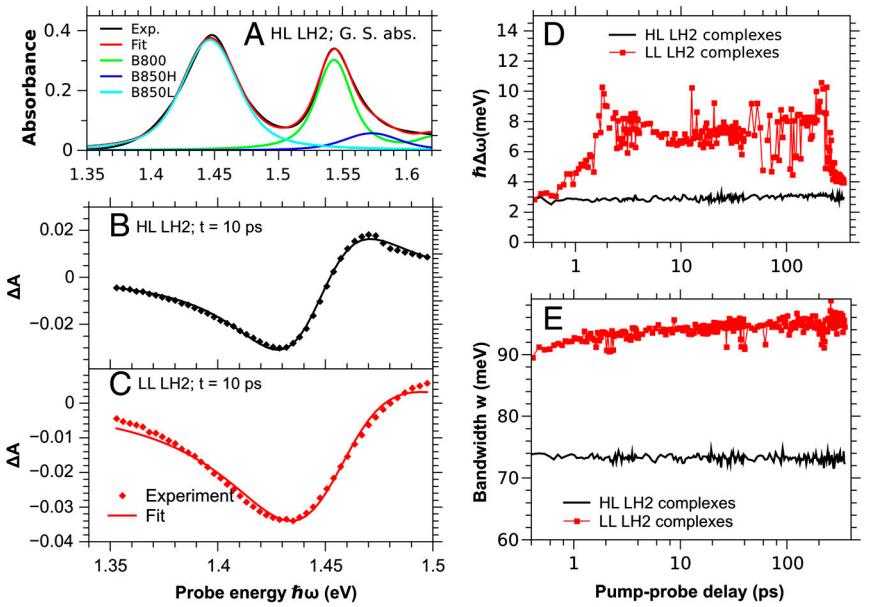

Fig. S2. (*A*) Ground-state absorption spectrum (G. S. abs.) of high light-grown LH2 complexes, and multi-Voigt fits. *B* and *C* show differential absorption spectra at 10 ps pump-probe delay for HL and LL LH2 complexes, respectively. Data points are given as diamonds. Black curves are fits by a superposition of two Lorentzians. The fitted offsets between the two Lorentzians, and the band widths (valid for both Lorentzians), are given in *D* and *E*, respectively.

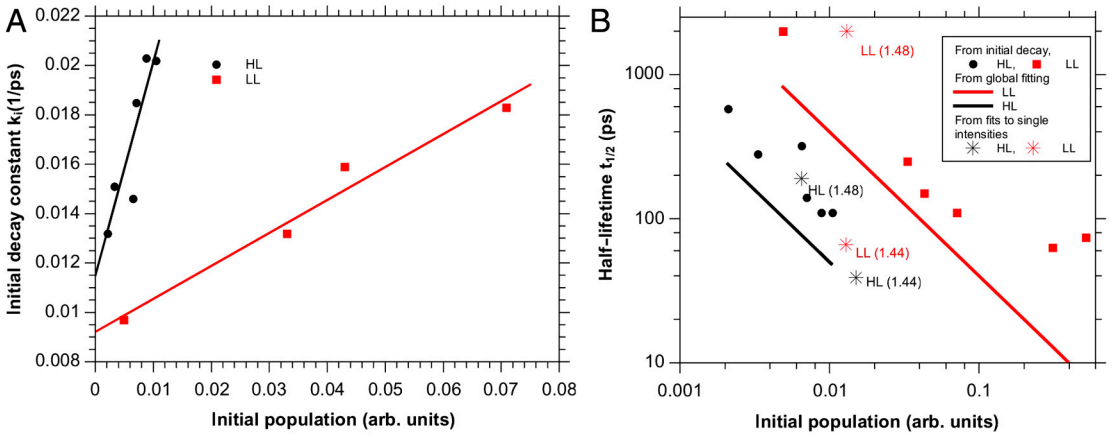

Fig. S3. (*A*) Initial decay constants according to Eq. **S8**, from fitting the initial part of B850 decay to an exponential model. Samples were HL and LL membranes pumped at 1.6 eV. Straight lines are linear regressions. (*B*) Bimolecular half-lifetimes $t_{1/2}$. Solid symbols, half-life times obtained according to Eq. **S4**. Pump energy 1.6 eV. Solid lines, half-lifetimes as obtained from a global fit for all intensities considering the full decay. Pump energy 1.6 eV. Stars, fitted values for the half-lifetimes of the measurements on which Table 1 in the main manuscript is based. Numbers in brackets are pumping energies in eV.